Electrocatalytic Hydrogenation of Furfural with Improved Activity and Selectivity at the Surface of Structured Copper Electrodes

Clément Spadetto[1], *Cyril Hachemi*[1], *Maxime Nouaille-Degorce*[1], *Loïc Pendu*[1], *Lou Bossert*[1], *Robert Temperton*[2], *Andrey Shavorskiy*[2], *Luis Cardenas*[1] *and Mathieu S. Prévot**[1]

[1] Univ. Lyon, Université Claude Bernard Lyon 1, CNRS, IRCELYON, 2 Av. A. Einstein, F-69626 Villeurbanne Cedex, France

[2] MAX IV Laboratory, Lund University, Box 118, 221 00 Lund, Sweden

KEYWORDS: Electrocatalytic hydrogenation, Furfural, Furfuryl alcohol, 2-methylfuran, Selective, High-pressure photoemission, In-situ

ABSTRACT

Furfural is a pivotal renewable platform molecule obtained from the chemical breakdown of cellulose. While it has traditionally been valorized to value-added chemicals through catalytic hydrogenation in biorefineries, its direct electrocatalytic hydrogenation presents attractive advantages. This article describes the significant improvements brought by the structuring of copper cathodes applied to this process, in terms of activity and selectivity. We show that structured electrodes are capable of converting furfural to furfuryl alcohol with 100% selectivity at potentials as high as - 0.2 vs. the reversible hydrogen electrode (RHE) in neutral conditions (pH 7.0). Moreover, the same electrode can selectively generate either furfuryl alcohol or 2-methylfuran in acidic conditions (pH 1.0), depending on applied potential and temperature. We further show the existence of optimal voltage-temperature conditions for the efficient conversion of furfural to furfuryl alcohol or 2-methylfuran, highlighting the delicate influence of operating conditions on the selectivity of furfural reduction, in competition with the hydrogen evolution reaction in aqueous electrolytes. These performances are attributed to the resilience of Cu (I) species under operating conditions and their likely contribution to the electrocatalytic active site, as revealed by quasi-in-situ photoelectron spectroscopy.

INTRODUCTION

The defossilization of the chemical industry requires both to transition away from fossil fuels as a source of energy and to replace petrochemical processes with alternatives based on renewable carbon resources. In this context, the valorization of lignocellulose, the most abundant organic substance on the planet, is of high interest. To achieve its efficient chemical valorization, most common biorefinery models are built around a multi-stage scheme involving the separation of

lignin, cellulose, and hemicellulose (primary refining), followed by the breakdown of these polymeric compounds into small platform molecules (secondary refining) and finally the chemical upgrading of these platform compounds into value-added chemical feedstock or fuel.[1] Among these platform molecules, furfural (FAL) has been identified as a promising substrate for the production of strategic targets in the value chains of the chemical industry.[2] One attractive way to renewably perform FAL valorization is to use decarbonized electricity to directly power its electrocatalytic reduction, with the advantages of (i) mild temperature and pressure conditions, (ii) the use of water as a source of hydrogen rather than H_2, (iii) a potentially more efficient use of renewable electricity compared to electrically heated reactors, and (iv) the possibility of combining FAL reduction with an oxidation process of interest in a single reactor. These concepts can in fact be generalized for the development of electrochemical biorefineries for the sustainable production of fuels and chemicals.[3,4] Regarding FAL electroreduction, two main products are usually identified (see **Figure 1**): furfuryl alcohol (FOH), produced by the reaction of FAL with two protons and two electrons, and 2-methylfuran (2-MF), generated from the reaction of FAL with four electrons and four protons accompanied by the elimination of a water molecule.

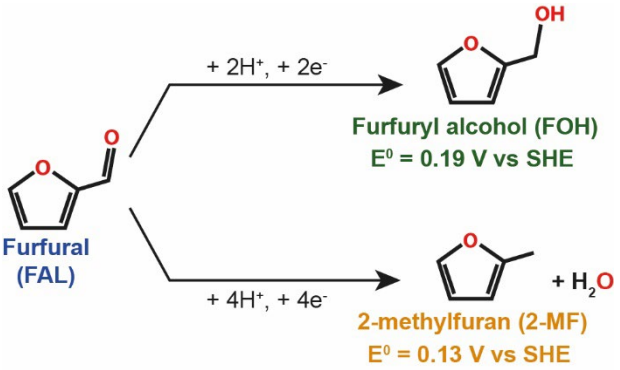

Figure 1. Electrochemical reduction pathways of furfural into furfuryl alcohol or 2-methylfuran. For each product the corresponding standard reduction potential is reported vs. the standard hydrogen electrode (SHE) from reference [5] where it was calculated from the corresponding Gibbs free energy of formation.

Finally, a third product is observed for higher concentrations of FAL: the hydrofuroin generated by the reductive coupling of two FAL molecules involving two electrons and two protons (not shown here). This latter product has traditionally been considered as less desirable, although it was recently proposed as a valuable precursor for the development of jet and rocket fuel.[6,7] While the first report on the electrocatalytic reduction, or electrocatalytic hydrogenation (ECH), of FAL dates back to 1939,[8] it has gained a renewed and rapidly growing interest over the last decade and has been the object of several recent perspective and review articles.[9–12] Early studies described the electrochemical reduction of FAL in aqueous media (sometimes containing methanol) inside H-cell setups, on a range of metal electrodes – Pt, Ni, Cu, Al, and stainless steel [13–16] – concluding that FOH is the major product in neutral and alkaline pH for all of these cathode materials, and the observation of 2-MF as a minor product (14% selectivity) at pH 1.0 on Ni.[15] In 2013, Nilges and Schröder reported for the first time the selective conversion of FAL to 2-MF in 0.5 M H_2SO_4 in a mixture of water and acetonitrile on Cu cathodes. In a seminal study published in 2017, Chadderdon et al. set out to study the mechanism of FAL electroreduction at the surface of Cu.[17] This work led them to conclude that FAL reduction was more likely to involve an electrochemical hydrogenation (ECH) pathway (i.e. adsorbed FAL molecules hydrogenated by neighboring adsorbed H atoms generated from proton reduction through a Volmer step), rather than the direct electroduction of adsorbed FAL from solvated protons through a proton-coupled electron transfer mechanism. The authors of this study also reported that FAL reduction occurred with a cathodic current onset at *ca.* - 0.35 V vs. the reversible hydrogen electrode (RHE) for a concentration of 0.05 M of FAL at pH 0.5 at the surface of Cu. The major product of the reaction was 2-MF for potentials ranging from -0.45 to - 0.65 V vs. RHE, the minor products being FOH and hydrofuroin. More negative potentials improved selectivity towards 2-MF but also favored the competing

hydrogen evolution reaction (HER). Moreover, lowering FAL concentration to 0.01 M prevented the production of hydrofuroin but also increased the preponderance of HER over FAL reduction. Finally, increasing the pH from 0.5 to 3.0 resulted in FOH becoming the major reduction product over 2-MF at - 0.55 V vs. RHE. Interestingly, the authors also demonstrated that 2-MF and FOH were produced through parallel rather than sequential pathways on Cu (as opposed to what is observed in thermocatalytic processes[18,19]). In 2016, Jung and Biddinger studied the influence of pH, solvent and FAL concentration on the activity and selectivity of FAL reduction.[20] They observed that varying the pH from 3.4 to 0 in a CH_3CN/water (20/80) solvent resulted in shifting the major product of the reaction from FOH to 2-MF, at -10 $mA.cm^{-2}$ (resulting in applied potentials ranging from -0.6 V to – 1.8 V vs. RHE) confirming the strong influence of pH on the selectivity of the reaction. The authors however indicated that they could not balance product generation and FAL consumption, pointing towards degradation or alternative pathways producing unidentified byproducts in their conditions. Moreover, they reported elsewhere that FAL reduction produced preferentially 2-MF in 0.5 M H_2SO4 + 0.1 M FAL with a faradaic efficiency (FE) of 35 – 60% for 2-MF and 10 – 25% for FOH between - 0.5 V and - 0.95 V vs. RHE, once again leaving a significant amount of unidentified byproducts out of the selectivity balance.[21] Finally, in a later study, they also reported the beneficial effect of Cu structuring by electrodeposition on FAL reduction in acidic conditions (improved FOH + 2-MF production compared to bare Cu).[22] A 2020 study from Anibal and Xu confirmed that FOH was selectively produced from FAL on Cu in neutral environments between - 0.5 and - 0.7 V vs. RHE,[23] while a 2021 report from Zhang and coworkers showed that single atom copper catalysts could switch from selectively producing FOH at - 0.75 V vs. RHE to selectively produce 2-MF at - 0.9 V vs. RHE in a pH 5 acetate buffer.[24] In 2022, the same group studied the reduction of FAL in 0.1 M acetic acid (pH 2.9) at the surface of

CuPd bimetallic electrocatalysts.[25] They measured a 75% FE for 2-MF in the presence of 0.04 M FAL at - 0.58 V vs. RHE, with a 100% selectivity (the remaining FE corresponding to H_2 evolution). For comparison, the same system generated 2-MF with a FE of only 21% in 0.1 M H_2SO_4 at the same potential. Improved performance compared to pure Cu were attributed to change in the adsorption mode of FAL and in the surface concentration of adsorbed H brought by the inclusion of Pd inside the catalyst lattice. Finally, a recent study by Xia et al. showed the ability of CuO nanowires grown on Cu to reduce FAL to FOH with a much lower overpotential than Cu in 1M phosphate buffer (pH not reported) + 0.05 M FAL.[26] Indeed, the authors report the selective conversion of FAL to FOH at potentials as high as – 0.2 V vs. RHE, and they attribute this performance to the resilience of some Cu(I) centers to the reductive operating conditions. This resulted in the formation of Cu(I)-Cu(0) active sites that displayed optimized FAL adsorption and FOH desorption properties, according to DFT modeling. Another study also pointed towards the beneficial effect of the presence of Ni^{2+} cations on the selectivity and activity of Cu electrodes towards 2-MF production in acidic media at – 0.45 V vs. RHE.[27] Regarding the mechanism of FAL reduction, a recent theoretical study published by Liu et al.[28] challenges the original claim of Chadderdon et al.[17] and argues that FAL reduction mainly proceeds through a PCET mechanism in acidic conditions and that surface hydrogenation and ECH only plays a minor role in the process. Finally, some research has been done to successfully implement electrocatalytic reduction of FAL to FOH in flow devices using Pd[5] and Cu[29] as cathode materials. Overall, despite significant progress achieved on Cu cathodes for FAL reduction, control over the selectivity of the process remains complicated, as 100% selectivity towards FOH or 2-MF is rarely achieved with the same material, and the potential applied in most studies (typically - 0.5 to - 0.7 V vs. RHE) indicate the presence of a high overpotential for this electrochemical process. Here, we tackle these

shortcomings and we report the beneficial effects of structuring copper electrodes by a self-templating electrochemical deposition on their performance towards electrocatalytic FAL reduction. We find that, in neutral phosphate buffer (pH 7.0), FAL can be reduced towards FOH with a 100% selectivity at potentials as high as - 0.2 V vs. RHE, representing a significant improvement over the typical potential of - 0.5 V vs. RHE required on Cu electrodes. We further show that, in acidic conditions (pH 1.0) we can direct FAL reduction with 100% selectivity towards either FOH or 2-MF at the surface of the same electrode, depending on the applied potential and the temperature of the electrolyzer. Under all conditions structured electrodes show improved current densities and comparable or better selectivity than polycrystalline copper foil. Surface characterization by UV and X-ray photoelectron spectroscopy, including in-situ measurements performed at the synchrotron, revealed the involvement of Cu(I) species in the electrocatalytic active site, even under reductive operating conditions. Overall, we present an easy and scalable strategy to produce active and selective copper electrodes for the electrocatalytic reduction of FAL towards 2-MF or FOH in aqueous media.

METHODS

Materials. Furfural (99%, Sigma-Aldrich), furfuryl alcohol (98%, Sigma-aldrich), 2-methylfuran (99% , contains 200-400 BHT as stabilizer), acetonitrile (HPLC-GOLD-Ultragradient grade, Carlo Erba), phosphoric acid (ACS Reagent ≥ 85%, Honeywell), potassium phosphate monobasic (≥ 99.0%, Sigma-Aldrich), potassium phosphate dibasic (ACS Reagant, ≥ 98%, Sigma-Aldrich), copper(II) sulfate pentahydrate (ACS Reagent, ≥ 98%, Sigma Aldrich), and sulfuric acid (ACS Reagant, 95.0-97.0%, Sigma Aldrich) were used without additional purification. An Elga PURELAB Option DV 25 provided the deionised (DI) water (ρ > 18.2 MΩ.cm). A commercial

Cu foil (0.25 mm thickness, 99.98% trace metal basis, Sigma-Aldrich) was used as the electrode substrate.

Cu electrodes preparation. Cu foil pieces cut to 3x1 cm^2 were cleaned thoroughly to remove surface contaminants before testing or electrodeposition. The Cu electrodes were first rinsed with DI water and acetone followed by a 10-min sonication step in acetone and an additional 10 min of sonication in DI water. The Cu foil pieces were dried at room temperature and ready for further electrochemical treatment. Self-templated structured Cu electrodes were produced according to a previously reported methodology.[30,31] Briefly, a current of 1 $A.cm^{-2}$ was applied between two pieces of copper foil immersed in an aqueous solution of 0.4 M $CuSO_4$ + 0.1 M H_2SO_4 for different durations using a 2-electrode setup powered by a RS-3005D (RadioSpare) power supply. The deposition time was varied between 10 and 60 seconds. An optimum was found for a deposition time of 40 seconds, corresponding to the maximal development of the porosity of the film, as additional deposited Cu tended to block the pores at longer deposition times (see **Figure S1)**. After electrodeposition, the structured Cu electrodes were carefully rinsed using DI water and soaked for 2 h in DI water to remove unreacted $CuSO_4$. Drying was performed on a hot plate at 60°C for 18 hours. Epoxy resin was then used to coat the electrode and roughly delimit a 1x1 cm^2 active surface area. A small area of pristine copper was left untouched to allow electrical contact with the circuit, but was not exposed to the electrolyte during electrochemical testing. The precise surface area of the electrode was measured each time using the software imageJ.

Electrochemical setup and experiments. A commercial air-tight jacketed H-type electrochemical cell (from DekResearch) was used throughout the study. The cell was double-jacketed and a Fisherbrand Polystat was used to control the temperature of the electrolyte. Both compartments of the cell were separated by a proton exchange membrane (Nafion® 117). The

anode compartment was filled with 0.1 M potassium phosphate (KPi) buffer or 1 M H_3PO_4 for the experiments performed at pH 7.0 and pH 1.0 respectively. FAL was only added to the cathode chamber at a concentration of 0.01 M. All electrochemical experiments were performed with a conventional three-electrode setup connected to a potentiostat (BioLogic SP-300). The Cu working electrodes and the Ag/AgCl reference electrode (3.5 M KCl) were located in the cathode chamber whereas the Pt coil counter electrode was placed into the anode chamber. The catholyte was continuously sparged with a 25 $mL.min^{-1}$ N_2 flow. This vector gas flowed any volatile and gaseous products through the outlet of the electrochemical cell into a cold trap (-10°C) filled with 15 mL of acetonitrile and cooled by a custom thermostated Peltier device, and sealed with a septum allowing for sampling. Thus, 2-methylfuran was collected in this acetonitrile cold trap, while H_2 and N_2 were analyzed in real time in a micro-gas chromatograph (INFICON Micro GC Fusion™). During kinetic measurement, the gas outlet was detached for less than a minute to collect samples using a syringe. Samples from the cold trap were directly taken through the septum without removing the cap. A scheme and photograph of the setup are provided in **Figure S2**.

Analysis of products. NMR experiments were performed by collecting 0.1 mL of electrolyte which was mixed with 0.4 mL D_2O in an NMR tube. Samples were then analyzed in a Bruker 400 MHz NMR spectrometer and data processed in TopSpin 3.6.5. A water peak suppression procedure was applied to each sample (see **Figure S11** for a representative spectrum). HPLC analysis was also performed to analyze liquid products. A Shimadzu High-Performance Liquid Chromatography (HPLC) system equipped with Phenomenex Synergi Hydro-RP column (150 × 4.6 mm) and a Photodiode Array UV-Vis Detector (SPD-M20A) was used. The HPLC analytical condition was set to a column temperature of 30 °C and 1 mL min^{-1} of mobile phase flow rate. Water acquired from an ELGA purelab option-Q purification system in which 0.5 v% H_3PO_4 was

dissolved (solvent A) and HPLC grade acetonitrile (solvent B) were used as mobile phase solvents. The nonlinear gradient of the two solvents was set to 100% A and 0% B at the start of the experiment and sequentially changed to 99% A and 1% B at 5 min, 80% A and 20% B at 6 min, 10% A and 90% B at 11 min and 100% A and 0% B at 14 min after injection. The total detection duration was 16 min. For a typical measurement, 500 µL of analyte was collected inside in a 2 mL HPLC vial. The results were taken at different wavelengths (210 nm for FAL; 230nm for 2MF and 232 nm for FOH) by the diode array detector. Identification of analytes was based on the retention time of the HPLC chromatogram while the quantification was done according to calibration curves (see **Figures S9 and S10**) and the ratio of peak areas between analyte and internal standard. The H_2 flow during the tests was quantified using the thermal conductivity detector of an INFINICON Micro GC Fusion™. N_2 was used as a carrier gas to transport H_2 into the micro GC for in-line analysis. The calibration of the system was performed using an electrochemical method: H_2 was produced at different current densities on a Pt foil and the quantity of produced H_2 was estimated using a 100% FE assumption.

X-Ray diffraction. The diffractograms of the electrodes were acquired with a Bruker D8 Advance A25 diffractometer using Cu Kα radiation (λ=0.154184 nm). Diffraction angles were scanned between 10 and 80°, and the signal was collected with a one-dimensional multistrip detector (Lynxeye, 192 channels on 2.95°)

Scanning electron microscopy (SEM). SEM images were recorded on a Zeiss Merlin Compact, using the secondary electron detector and an acceleration voltage of 5 kV, to document the surface morphology of the prepared electrodes.

X-Ray Photoelectron Spectroscopy (XPS). XPS analyses were conducted in an integrated ultrahigh vacuum system, connected to an Axis Ultra DLD spectrometer (Kratos Analytical). Spectra were recorded with a monochromatic Al Kα source (hν=1486.6 eV) operated at a nominal power of 150 W (10 mA x 15 kV). The pass energy was set to 160 eV for wide scans and 40 eV for core levels and Auger lines. The binding energy scale was calibrated with the C 1s of adventitious carbon (284.6 eV). The data were treated using IGOR Pro Software (Wavemetrics Inc.). Peaks were fitted with Voigt functions and a Shirley background. For quasi-in-situ experiments, a portable glove box filled with N_2 was used to conduct the electrochemical experiment. The electrochemical cell was installed inside the glove box while cables from the potentiostat were introduced through a tight aperture, properly sealed to prevent air leaks inside the glove box. The glove box was under constant N_2 flow during the experiment. When the electrochemical test was over, the working electrode was removed from the cell, quickly rinsed and dried on a Kimtech wipe and transferred through an airlock directly from the glove box to the XPS sample chamber, before being put under vacuum and tested. Photographs of the glove-box setup are provided in **Figure S3.**

In-situ XPS experiment at MAX IV facilities (HIPPIE beamline). These experiments were carried out at the HIPPIE beamline of the MAX IV Laboratory. Electrochemical experiments were performed using the electrochemical cell available at the beamline, equipped with a three-electrode setup connected to a Bio-Logic SP-200 potentiostat located outside of the instrument. The beamline is equipped with a Scienta HIPP-3 analyzer, with an entrance cone of diameter ~0.15 mm, positioned in the horizontal plane at a 55° angle of the X-ray beam (set to linear-horizontal polarization). An incident photon energy of 1600 eV was used to collect Cu 2p and C 1s spectra and the projected spot size on the sample was ~100x25 μm^2. The working electrode was a 2x1 cm^2

piece of copper foil, the counter electrode was a Pt wire (diameter 0.3 mm) and the reference electrode was Ag/AgCl/KCl (eDAQ ET072). All three electrodes were held by a manipulator set at the top of the XPS chamber. A beaker containing 1M H_3PO_4 (degassed in a separate vacuum chamber prior to use in the XPS instrument) and 0.01 M of furfural when needed, was supported on another manipulator located at the bottom of the chamber. Under operation the equalized chamber pressure was in the 12-15 mbar range after pumping down. For each measurement, a chronoamperometry was performed with all three electrodes immersed in the electrolyte at a given applied potential for 30 min. At the end of the experiment, the electrodes were pulled out of the electrolyte, leaving a thin layer of liquid at the surface of the working electrode. This working electrode was then approached to a distance of ~0.3 mm of the analyzer to acquire the XPS data. The electrodes were then immersed again in the electrolyte before proceeding to the next chronoamperometry.

RESULTS AND DISCUSSION

Standard characterization

The composition and morphology of the templated electrode was investigated by XRD, XPS and SEM. The XRD data acquired for the electrodeposited copper and for the Cu foil substrate are displayed in **Figure 2a**. The diffractogram of the Cu foil only showed crystalline face-centered cubic Cu(0) with preferential orientation along the {200} range of planes. Conversely, the diffractogram of the structured electrode showed reduced texturing of the Cu(0) phase compared to the pristine foil, and the presence of a Cu_2O phase that did not exhibit strong preferential orientation along any diffraction plane. This indicated that the electrodeposited layer contained randomly oriented Cu(0) and Cu_2O crystals. The morphology of these crystals was then monitored by SEM. **Figure 2b** shows a picture of the typical surface observed for a structured electrode

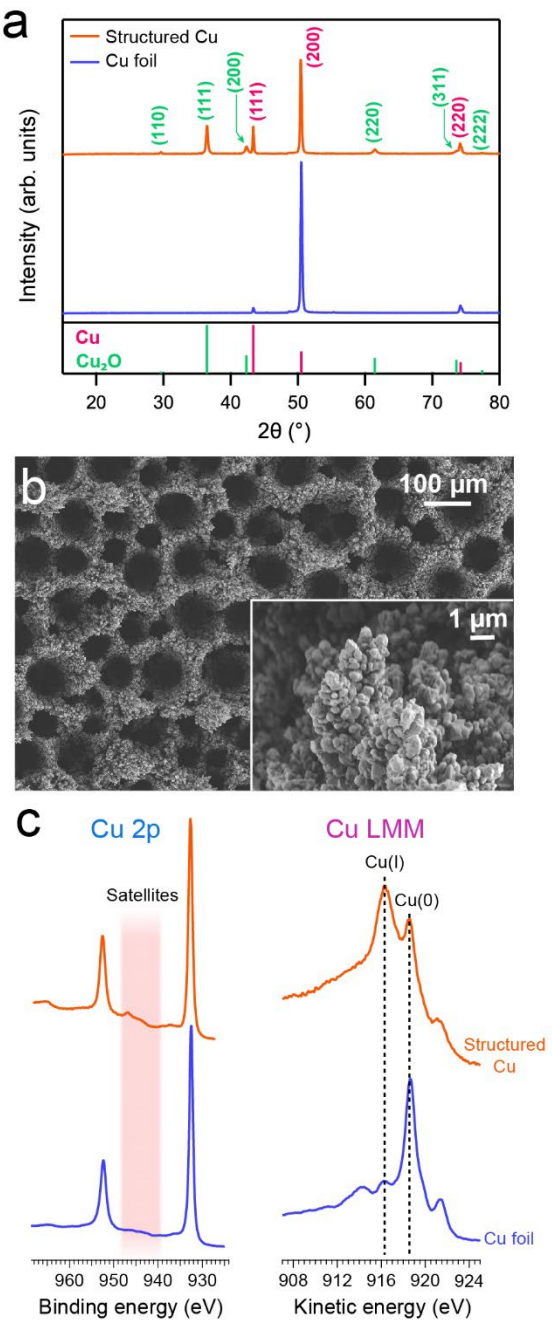

Figure 2 a) XRD data obtained on the electrodeposited Cu electrode and on the Cu foil substrate. b) Low-magnification SEM picture of the self-templated porous copper electrode Inset: higher magnification SEM picture showing the morphology of electrodeposited Cu microcrystals. c) Cu 2p and Cu LMM XPS spectra measured on bare copper foil and on a structured electrode obtained after 40 seconds of electrodeposition.

obtained after a deposition time of 40 seconds. A hierarchical architecture was observed: the electrodeposited layers contained microcrystals (in the 100 nm – 1 µm size range) grown around micropores of 10 – 100 µm in diameter, generated by the concurrent evolution of H_2 bubbles during the electrodeposition process. Finally, the chemical compositions of the surface of both the foil and the structured electrode were probed by means of ex-situ XPS. The Cu 2p and Cu LMM signals are displayed in **Figure 2c.** They show that the surface of the copper foil was expectedly mostly composed of Cu(0), as evidenced by the main Cu 2p peak at 931 eV and the secondary peak at 951 eV in binding energy (BE), stemming from spin-orbit splitting, accompanied by the Auger peak at 918.5 eV in kinetic energy (KE). The presence of faint satellite peaks between 940 and 950 eV in BE in the Cu 2p spectrum and a small Auger peak at 916.5 eV in KE indicated the presence of a small amount of Cu(I) at the surface of the copper foil. In contrast, the XPS spectra of the electrodeposited structured layer show a more pronounced signal for Cu(I) species – satellite peaks in the Cu 2p spectrum and an intense Auger peak at 916.5 eV in KE – revealing that the Cu_2O phase identified by XRD was present at the surface of the freshly structured electrode. Finally, an increase in electrochemical surface area (ECSA) of a factor 15 was found between the bare Cu electrode and the structured one (see **Figure S4** and **S5**). However, on the structured Cu, we anticipate that part of the ECSA is hardly accessed by furanic species due to diffusion limitations.

Electrochemical conversion of furfural in neutral pH

The structured copper film was tested as cathode for the reduction of FAL in a three-electrode electrochemical cell (see **Figure S2**). First, cyclic voltammetry (CV) experiments were performed at different temperatures. For each temperature, a CV was acquired on the Cu foil and on the electrodeposited structured Cu electrode, first with both the anode and cathode compartments filled with 0.1 M KPi buffer at pH 7.0, and then with the cathode compartment filled with the same 0.1

M KPi buffer to which was added 0.01 M of FAL. This FAL concentration was chosen to prevent the formation of hydrofuroin byproducts, observed at higher concentrations and complicating the study at hand, while providing limited added value to it. In the absence of FAL, the CV of the Cu foil appeared essentially featureless at all temperatures, with a reduction current onset occurring at - 0.6 V vs. RHE, attributed to the HER. On the contrary, the CV of the structured electrode showed two reduction waves at all temperatures. The first one was observed at + 0.38 V vs. RHE and attributed to the reduction of Cu(II) species, and the second one at - 0.40 V vs. RHE and was attributed to the reduction of Cu(I), coexisting with and prolonged by the HER wave at more negative potentials.[32] The CV scans displayed in **Figure 3** correspond to a stable measurement over multiple cycles, typically obtained after two initial CV scans in which a large quantity of surface oxidized copper is reduced (see **Figure S6**). The fact that the reduction wave at - 0.40 V vs. RHE remained part of the stable CV signal indicated that some Cu(I) remained steadily electrochemically accessible in the range of monitored potentials. Once FAL was added to the electrolyte, an increase in reduction current was observed both for the Cu foil and the structured Cu. On Cu foil, the reduction current onset was shifted positively by about 0.1 V (thus occurring at – 0.5 V vs. RHE) at all temperatures, indicating the kinetically easier reduction of FAL on Cu compared to the HER. Moreover, a plateau current varying from about - 2 to - 4 $mA.cm^{-2}$ between 20°C and 50°C and measured at - 0.7 V vs. RHE was associated with FAL reduction on bare Cu foil. This agreed with previous reports.[11,17] On the structured electrode, a similar slight positive shift in the onset of reductive currents was observed, but this time, it was accompanied by a much higher increase in current density forming a reduction wave in the potential range where the reduction of Cu(I) occurred. Because this increase in reduction current was directly linked to the presence of FAL in the electrolyte, it was attributed to the reduction of FAL (indicated by an arrow

in **Figure 3**). Additionally, a small oxidation wave appearing between - 0.2 and + 0.2 V vs. RHE in the presence of FAL was tentatively attributed to the re-oxidation of adsorbed reduction products on the surface of the electrode. Importantly, according to these CV measurements and their proposed interpretation, the onset of FAL reduction on structured Cu electrodes was measured at - 0.16 V vs. RHE at 20°C, and reaching values as high as - 0.10 V vs. RHE at 50°C. To confirm the ability of structured Cu to reduce FAL at such low overpotentials and to study the selectivity of the process, chronoamperometry (CA) measurements coupled with product identification and quantification were performed at several potentials (- 0.2, - 0.3, - 0.4 and - 0.5 V vs. RHE) and temperatures (20°C, 30°C, 40°C and 50°C). The results obtained after 1 hour of CA under each condition are presented in **Figure 3e**. While no product was detected after one hour at - 0.2 and - 0.3 V vs. RHE at 20°C and 30°C, when the temperature was raised to 40°C and above, FOH was generated with an FE of 100%. Furthermore, FOH could also be generated with a 100% FE at - 0.4 V vs. RHE at 20°C. Higher temperatures and more negative potentials resulted in the apparition of H_2 as a competing reduction product from HER. Under all conditions, FOH was selectively produced from the reduction of FAL as no other product was detected by NMR, HPLC or micro-GC. Interestingly, when the same experiment was performed on Cu foil, negligible current densities and no FAL conversion were measured after 1 hour of polarization at - 0.5 V vs. RHE (see **Table S1**), highlighting the significantly improved electrocatalytic properties of structured Cu electrodes compared to the performance of Cu foil reported here and in previous works, as we show that our structured Cu electrodes can selectively convert FAL to FOH with a 100% FE at minimal overpotential. To investigate the kinetics of the process, FAL reduction was conducted on structured Cu electrodes at - 0.5 V vs. RHE and at 20°C, 30°C, 40°C and 50°C.

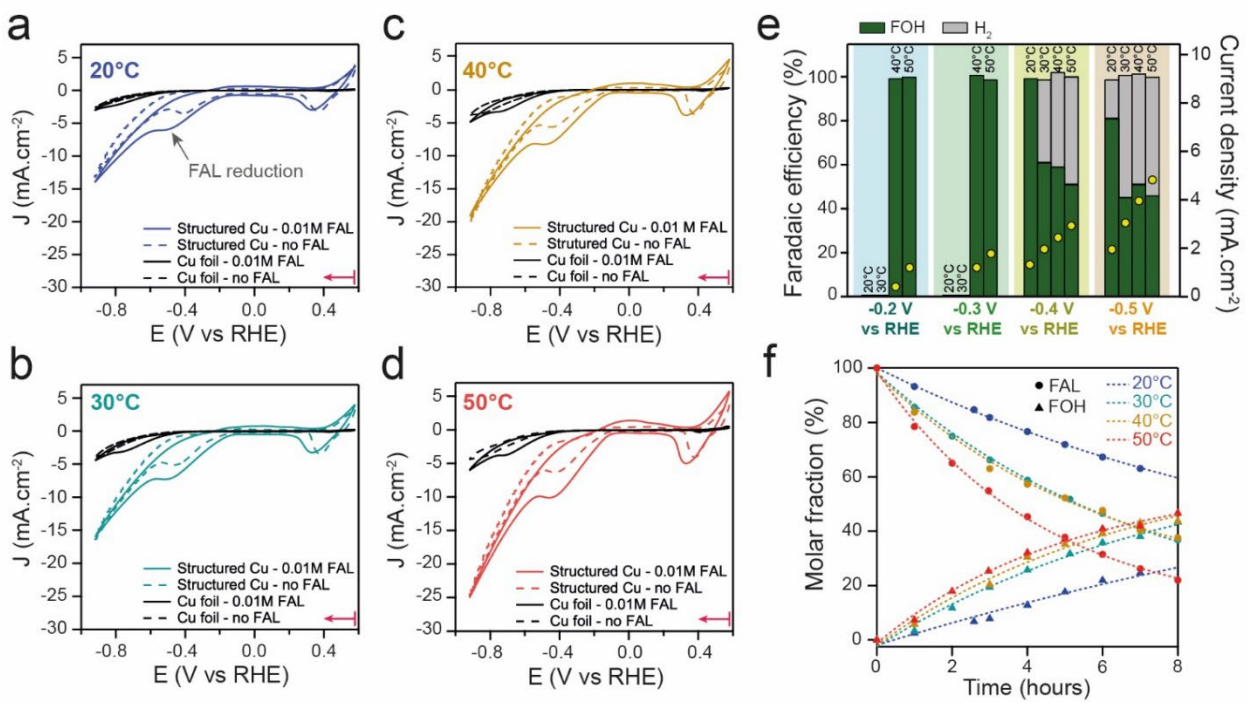

Figure 3 Cyclic voltammograms obtained for Cu foil and a structured Cu electrode in the absence (dotted trace) and presence (solid trace) of 0.01 M FAL at various temperatures: a) 20°C, b) 30°C, c) 40°C, and d) 50°C. Electrolyte: 0.1 M KPi buffer (pH 7.0). Scan rate: 20 $mV.s^{-1}$ (the pink arrow indicates the origin and direction of the CV scan). All measurement performed under N_2 sparging (25 $mL.min^{-1}$). e) Values of faradaic efficiencies measured after 1 hour of chrono-amperometry using structured Cu electrode as working electrode in a 0.1 M KPi + 0.01 M FAL (pH 7.0) electrolyte at temperatures varying from 20°C to 50°C and applied potentials varying from - 0.2 to - 0.5 V vs. RHE, indicated on the left Y axis. Green bars correspond to FOH production and grey bars correspond to H_2 production. Yellow markers indicate the average current density measured during the chronoamperometry and their value are referenced to the right Y axis. f) Measured molar fraction of organic compounds collected over time, for an applied potential of - 0.5 V vs. RHE in a 0.1M KPi + 0.01 M FAL (pH 7.0) electrolyte, and at various temperatures. Only FOH and FAL were detected by HPLC and NMR throughout the course of the experiment. The markers represent experimental data, while dotted lines correspond to their fitting with a first-order kinetic model.

The results of this experiment are shown in Figure 3f. Over the course of the experiment no other FAL reduction product than FOH was detected. The conversion of FAL to FOH was found to follow an apparent first-order kinetic law at all temperatures, with a typical increase in the rate of reaction with the temperature. However, as the temperature was increased, increasingly noticeable amounts of FAL evaporated from the electrolyte over time, carried away by the sparging N_2 flow. This explains the difference .in apparent rate between FAL consumption and FOH production at 50°C in **Figure 3f**. When fitted with the Arrhenius equation, the kinetic data obtained for FOH production afforded an apparent activation energy of 23 $kJ.mol^{-1}$ (see **Figure S7**). This value was found comparable to what others measured for catalytic aldehyde hydrogenation towards alcohol in thermochemical or electrochemical setups.[33–36] Considering the experimental setup employed in this study (unstirred batch H-cell and low FAL concentration), one could argue that diffusion kinetics were limiting. However, quasi in-situ XPS data presented in a later section (see **Figure 5**) suggest that FAL conversion is limiting, as the surface of the electrode is mostly covered in FAL under operating conditions. Overall, these experimental results prove that FAL can be selectively converted to FOH at much improved overpotential on the surface of structured Cu electrodes under neutral conditions and at temperatures below 50°C.

Electrochemical conversion of furfural in acidic pH

It is well known that pH has a strong influence on FAL reduction selectivity at the surface of copper, with an increased selectivity towards 2-MF over FAL at low pH.[10] While most studies have been conducted in H_2SO_4 electrolytes, we chose to employ H_3PO_4 as a source of protons, so as to keep the same counter anion (PO_4^{3-}) as in our study in neutral conditions (in which the electrolyte was buffered with potassium phosphate salts). Thus, the following experiments were conducted in a 1M H_3PO_4 solution exhibiting a pH of 1.0. First, CV were collected for Cu foil and structured

Cu electrodes at 20°C, 30°C, 40°C and 50°C in the absence and presence of 0.01M FAL. The resulting curves are shown in **Figure 4a-d**. They revealed that, in acidic conditions, both Cu foil and structured Cu generated much higher current densities that in neutral pH, indicating a drastic promotion of HER on Cu electrodes at low pH. Interestingly, while the onset of HER was observed at - 0.50 V vs. RHE on Cu foil, it shifted to - 0.30 V vs. RHE on the structured electrode, resulting in significantly improved electrocatalytic HER activity, and thus to increased current densities, for the structured film over the foil. Moreover, contrary to what was observed in neutral conditions, no defined feature was observed in the CV of either the Cu foil or the structured Cu, indicating that once reduced over the first CV scan (see **Figure S6**), the surface oxide layer was not electro-active in this range of potentials. When FAL was introduced in the electrolyte, a slight positive shift of a few tens of mV in onset potential was observed on Cu foil at all temperatures. On the structured electrodes, the introduction of FAL also resulted in a minor shift in onset potential, but, this time, also accompanied by the appearance of a reduction wave located at the foot of the HER wave. This reduction wave, located roughly between - 0.30 and - 0.35 V vs. RHE at all temperatures was thus attributed to FAL reduction. Interestingly, as the temperature increased, this FAL reduction wave was increasingly merged with the HER wave, suggesting a different influence of temperature on the reduction kinetics of water and FAL in 1M H_3PO_4. Compared to what was observed under neutral conditions, there was significantly less change in electrochemical activity upon addition of FAL, indicating a stronger competition between the HER and FAL reduction. Again, 1-hour CA experiments were performed at - 0.3, - 0.4, - 0.5 and - 0.6 V vs. RHE, each at 20°C, 30°C, 40°C and 50°C in 1M H_3PO_4 + 0.01 M FAL on the Cu foil and on the structured electrode. Importantly, 2-MF, because of its low solubility in water and relatively high volatility,

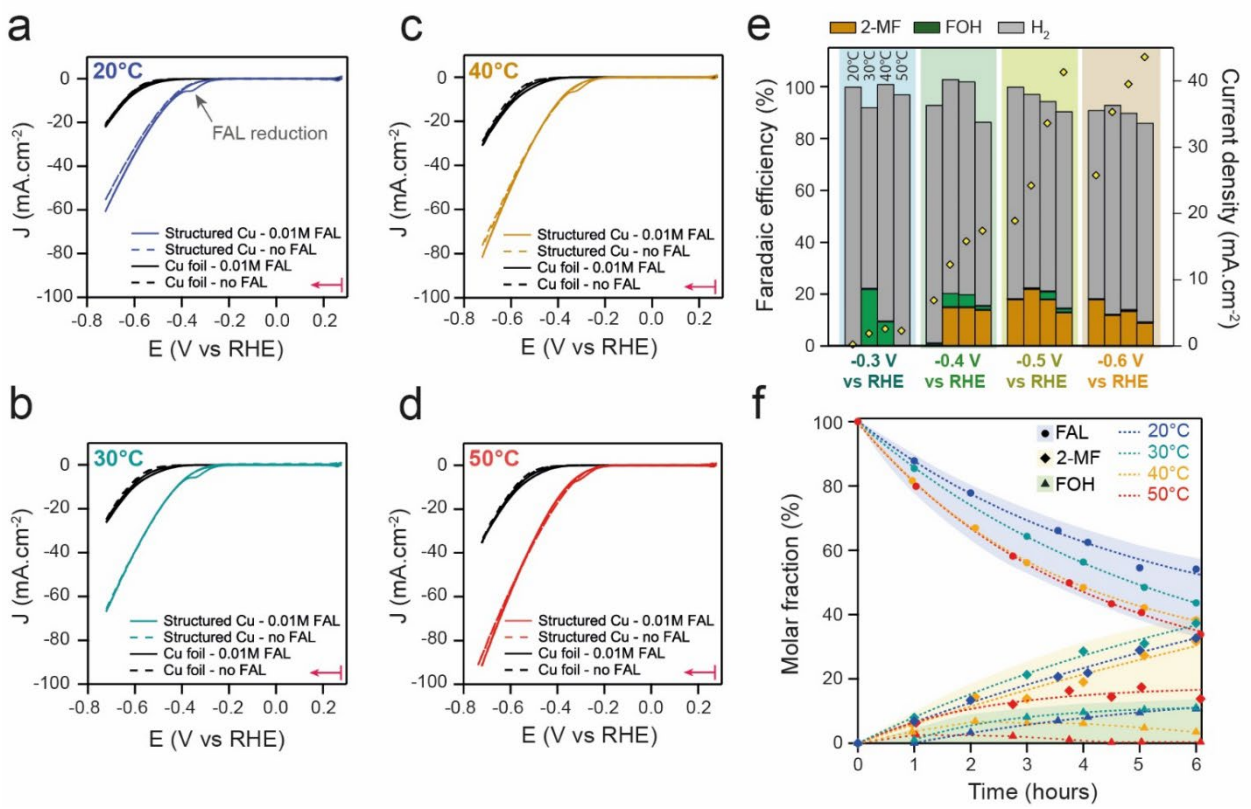

Figure 4 Cyclic voltammograms obtained for Cu foil and a structured Cu electrode in the absence (dotted trace) and presence (solid trace) of 0.01 M FAL at various temperatures: a) 20°C, b) 30°C, c) 40°C, and d) 50°C. Electrolyte: 1 M H_3PO_4 (pH 1.0). Scan rate: 20 $mV.s^{-1}$ (the pink arrow indicates the origin and direction of the CV scan). All measurement performed under N_2 sparging (25 $mL.min^{-1}$). e) Values of faradaic efficiencies measured after 1 hour of chrono-amperometry using structured Cu electrode as working electrode in a 1 M H_3PO_4 + 0.01 M FAL (pH 1.0) electrolyte at temperatures varying from 20°C to 50°C and applied potentials varying from -0.3 to -0.6 V vs. RHE, indicated on the left Y axis. Green bars correspond to FOH production, orange bars to 2-MF production and grey bars to H_2 production. Yellow markers indicate the average current density measured during the chronoamperometry and their value is referenced to the right Y axis. f) Measured molar fraction of dissolved organic compounds in the electrolyte and in the cold trap over time, for an applied potential of - 0.5 V vs. RHE in a 1M H_3PO_4 + 0.01 M FAL (pH 1.0) electrolyte, and at various temperatures. Only FOH, 2-MF and FAL were detected by HPLC throughout the course of the experiment. The markers represent experimental data, while dotted lines correspond to their fitting with a first-order kinetic model for FAL and 2-MF, but only serve as a guide for the eye for FOH, as it decomposes over time.

tended to rapidly leave the electrochemical cell, carried away by the N_2 stream (something that was not observed with FOH). Therefore, to quantify 2-MF production, a cold trap, consisting of CH_3CN cooled down to -10°C by a Peltier device, was installed at the outlet of the working electrode compartment of the electrochemical cell. 2-MF was recovered in this trap and quantified by HPLC measurements, whereas FOH was collected and measured inside the working electrode compartment (similar to under neutral conditions). Finally, H_2 evolution was quantified by a micro-GC connected in-line with the outlet of the cold trap (see **Figure S2**). For all measurements, a total FE in the 87 - 106 % range was obtained, which was considered acceptable, given the diversity of collection and analysis techniques required to quantify all the products. The FE measured on the structured Cu after each CA are displayed in **Figure 4e**. At - 0.2 V vs. RHE, at all temperatures, very low current densities (below 0.1 $mA.cm^{-2}$, not shown in **Figure 4e**) were measured and only traces amount of H_2 were detected, in contrast with what was observed in neutral conditions. When the potential of the working electrode was shifted to - 0.3 V vs. RHE at 20°C, similarly low current densities were measured and only H_2 was detected as a product. However, FAL conversion was observed and found to be selective towards FOH at 30°C and 40°C. Further increasing the temperature from 30°C to 40°C at this potential led to an increase in H_2 production, but did not affect the selectivity of FAL reduction, which remained 100% directed towards FOH. Interestingly, increasing the temperature to 50°C further favored the HER to the point of preventing FAL reduction altogether. This indicated that, at - 0.3 V vs. RHE, increasing the temperature improved the kinetics of both FAL reduction and HER, but that the HER was kinetically more favored at high temperature, leading to an optimum for FAL reduction at around 30°C. When subjected to - 0.4 V vs. RHE, the structured Cu was once again capable of reducing FAL only at temperatures above 30°C, despite significant current densities drawn at 20°C,

showing that HER proceeded more easily than FAL reduction at this temperature. However, at this potential and above 30°C, the selectivity of FAL reduction was preferentially directed towards 2-MF, although a significant amount of FOH was also detected as secondary product. Once again, when the temperature was raised from 30 to 40 and finally 50°C, FAL reduction was increasingly more disfavored compared to HER, but interestingly the FE towards 2-MF was not affected and remained quasi-constant at around 15%, indicating that temperature affected both reduction pathways differently. Indeed, at - 0.4 V vs. RHE, the increase in H_2 production was exclusively achieved to the detriment of FOH production (similarly to what was observed at - 0.3 V vs. RHE). Finally, at - 0.5 V vs. RHE, a much better selectivity for 2-MF was achieved, since a 100% conversion towards 2-MF from FAL was observed at 20°C and 30°C, while only a few percent of FOH were detected at higher temperature. At this potential, an optimal activity for 2-MF production was measured at 30°C, where a FE of 22% was obtained for 2-MF and no FOH was detected. When subjected to the same conditions, Cu foil only produced very small current densities, making the accurate quantification of products and the calculations of FE difficult with our experimental setup, although we can report that only 2-MF and H_2 were detected as products (see **Table S2**). Kinetics measurements were performed at - 0.5 V vs RHE for temperatures of 20°C, 30°C and 40°C and the results are presented in **Figure 4f**. As expected, an increased rate of FAL reduction was measured with increasing temperature. Attempt at calculating the apparent activation energy of the process based on the kinetics of 2-MF production resulted in a non-Arrhenius behavior (see **Figure S8**). This independence on temperature was ascribed to the process being limited by FAL diffusion to the surface of the electrode, which was confirmed by quasi in-situ XPS measurements (see **Figure 5c**), showing that the surface of the electrode was covered in reduction product under operating conditions. This also contributed to explain the preponderance

of HER under these conditions, and we suspect that much improved FE could be obtained with an optimized cell geometry. Furthermore, it appeared that, contrary to what the data presented in **Figure 4e** and collected after only one hour may suggest, FOH was ultimately produced at all temperatures, but with a temporal delay compared to 2-MF, indicating a change in the environment of the electrocatalytic site over time. We rationalize this behavior by suggesting that as HER and FAL proceed at the surface of the electrode, the consumption of protons shifts the local pH towards higher values, in turn shifting the selectivity of FAL reduction towards FOH production. This is consistent with the observation that FOH production occurs sooner at higher temperatures, at which higher current densities indicate faster proton consumption and therefore faster increase in the local pH. Finally, we observe that the concentration of generated FOH decreases over time, indicating chemical degradation of this compound in acidic media, which was confirmed by NMR analysis, revealing that the furanic ring underwent an opening, leading to the formation of a non-identified non-aromatic degradation product identified (see **Figure S12**). The results presented in **Figure 4** demonstrate the possibility to tune the selectivity of FAL reduction as a function of applied potential and temperature, and show that the selectivity of the process is highly sensitive to the local environment of the active site. We believe in particular that the local pH can quickly change under operating conditions, resulting in shifts in selectivity over time. Overall, despite the preponderance of the HER under the conditions of this study, we demonstrated that FAL could be converted in 1M H_3PO_4 at potentials as high as - 0.3 V vs. RHE and achieve complete initial selectivity towards FOH at -0.3 V vs. RHE (although the product quickly degrades) and towards 2-MF at - 0.4 V vs. RHE and below.

Photoelectron spectroscopy analysis

To understand the difference in activity and selectivity between our structured electrodeposited copper electrode and the copper foil, we resorted to photoelectron spectroscopy. First, quasi-in-situ XPS experiments were performed, in which a structured electrode was subjected to electrolysis conditions (in neutral or acidic electrolyte) in the presence of FAL for 30 min at - 0.5 V vs. RHE, and quickly transferred under inert atmosphere to the XPS chamber for analysis (see the Methods section). The acquired Cu 2p and Cu LMM spectra are shown in **Figure 5a**. The spectral signature of Cu(I) – satellites peaks and shoulder at 934 eV in the Cu 2p spectrum and the peak at 916.5 eV in KE in the Cu LMM spectrum – revealed that surface Cu(I) existed at the surface of the electrode under operating conditions at both pH. The corresponding C 1s spectra are displayed in **Figure 5b**, exhibiting several peaks and thus indicating the presence of different carbon species at the surface of the electrode. Under acidic conditions, the main peak at 284.6 eV was attributed to C-C and C-H bonds, while the smaller peak at 286.1 eV was attributed to C-O bonds. In neutral conditions, the same two signals were observed, plus one small peak at 288.5 eV, attributed to C=O bonds, and finally a shake-up peak at 292.9 eV, attributed to aromatic carbons.[37] These signals are thus generally consistent with the spectral signatures of FAL and its reduction products adsorbed at the surface of the electrode. We note that because of the lower signal-to-noise ratio obtained in acidic conditions, it is probable that the small C=O and aromatic shake-up signals exist but are within the noise of the measurement. To gain insight into the nature of the adsorbed chemicals, the atomic contribution of each of the aforementioned XPS peaks to the entire spectrum have been measured and are displayed in **Figure 5c**. In acidic conditions, we calculated an 80/20 ratio for the C-C/C-H over C-O bond signals. This composition is close to the theoretical composition of 2-MF (83/17) and suggests that the surface of the electrode is mostly covered in

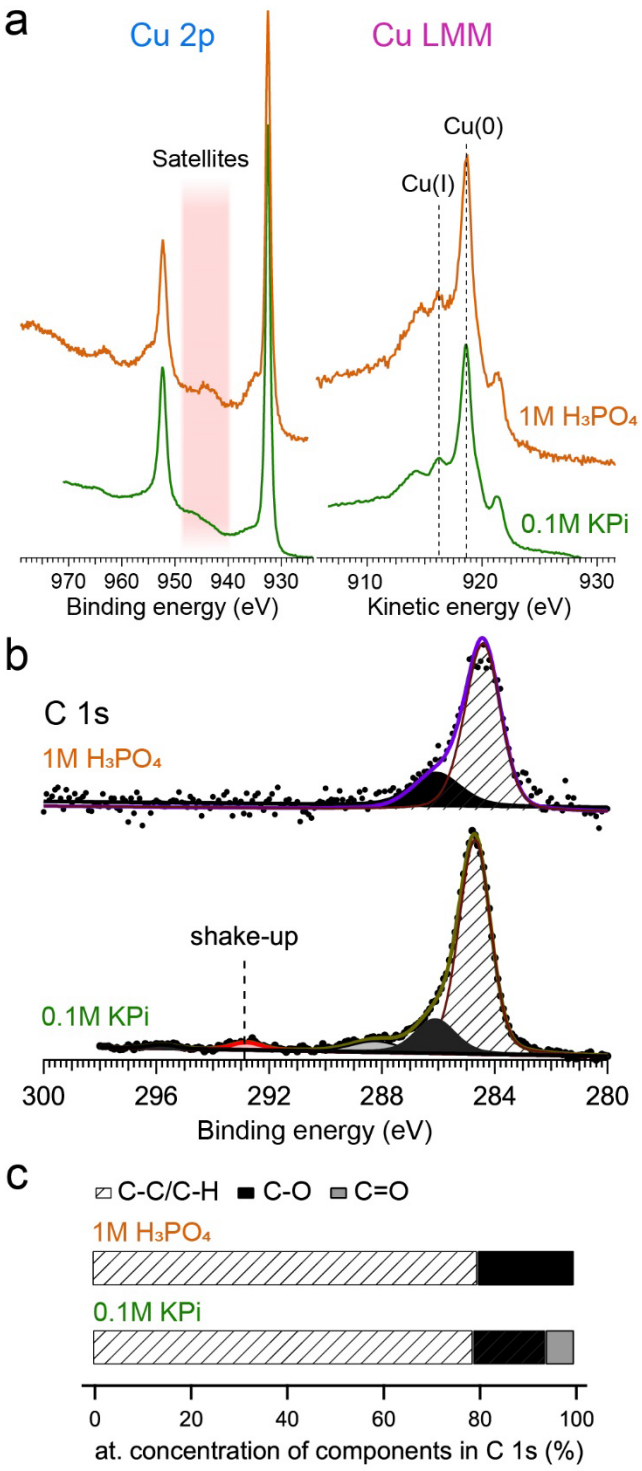

Figure 5 a) Cu 2p and Cu LMM XPS spectra measured on structured electrodes under quasi in-situ conditions after 30 min of electrolysis at – 0.5 V vs. RHE in 1M H_3PO_4 (orange trace) or 0.1M KPi (green trace) containing 0.01M FAL. b) C 1s spectra measured after 30 min of electrolysis at

– 0.5 V vs. RHE in 1M H_3PO_4 (top graph) or 0.1M KPi (bottom graph) containing 0.01M FAL. c) Atomic percent of C 1s components extracted from spectra displayed in b.

reduction products. On the other hand, in neutral conditions, a 79/15/6 distribution for C-C/C-H, C-O and C=O bonds respectively rather suggests a significant coverage of FAL (theoretical distribution of 72/18/9) molecules on the surface of the electrode at the end of the electrolysis. This led us to conclude that FAL is rapidly reduced once adsorbed on the surface of the electrode in acidic conditions, making the process diffusion limited, while it is converted more slowly in neutral conditions and therefore tends to accumulate on the surface of the electrode in neutral conditions, suggesting the process is limited by the electrochemical reaction. To further approach operating conditions with our spectroscopy measurements, we set out to perform proper in-situ XPS experiments at the HIPPIE beamline of the MAX IV synchrotron light source in Lund, Sweden.[38] Briefly, it consisted in performing XPS measurements directly at the surface of a working electrode connected to a three-electrode setup immersed in a liquid electrolyte inside an analysis chamber pressurized at 12-15 mbar (see Methods section for more details). Unfortunately, because the structured electrodes were rapidly soaked by the electrolyte, the signals of interest (Cu 2p and C 1s) were masked by the water signal and they could not be analyzed under this configuration. Still, in-situ XPS measurements were performed on copper foil that presented suitable wettability. Moreover, 1M H_3PO_4 was chosen as the electrolyte, because of the rapid precipitation of KPi at the surface of the electrode during the acquisition of in-situ XPS data. The CV obtained on the copper electrode inside the XPS chamber is displayed in **Figure 6**. A first series of measurements was conducted in pure 1 M H_3PO_4 electrolyte. The Cu 2p XPS spectrum of the electrode surface was measured at several potentials from + 0.2 V to - 0.5 V vs. RHE. The results are shown in **Figure 6c**. They revealed that, while Cu(II) species existed at potentials higher

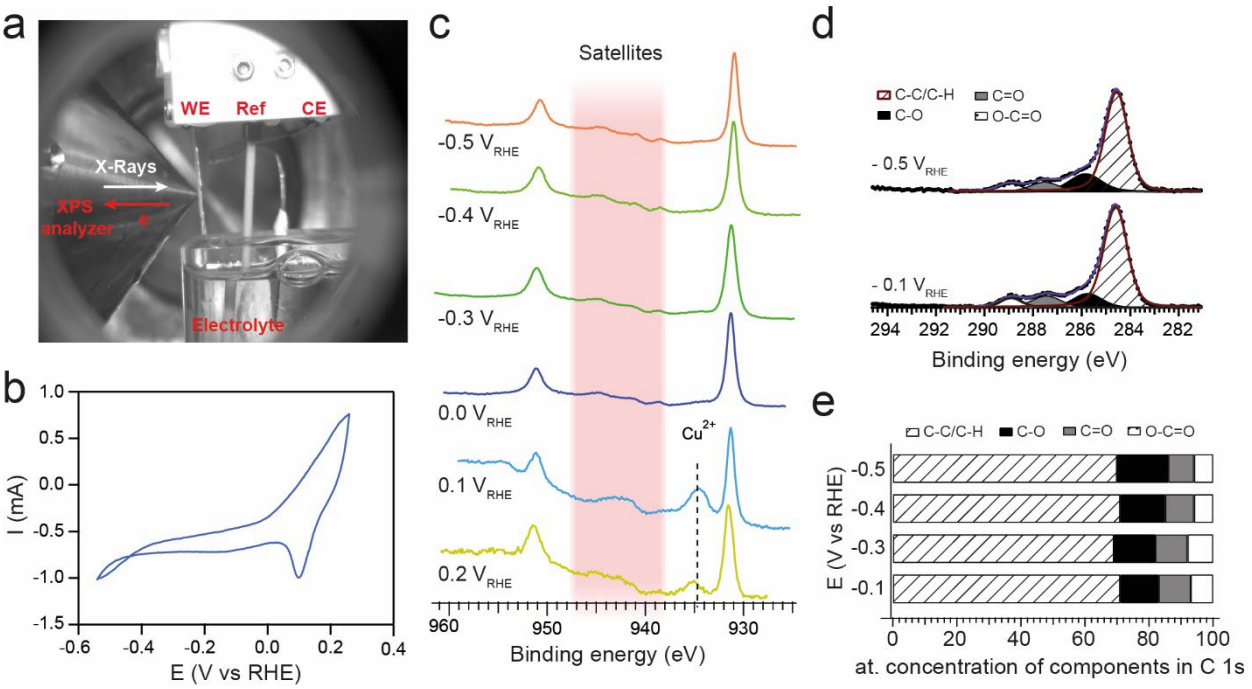

Figure 6 a) Photograph picture of the experimental three-electrode setup inserted inside the XPS chamber on the HIPPIE beamline at the MAX IV light source facility. b) Cyclic voltammetry acquired with the setup pictured in a, on a copper foil immersed in a 1 M H_3PO_4 electrolyte containing 0.01 M of FAL. c) In-situ Cu 2p spectra acquired at different potentials for a copper foil immersed in 1 M H_3PO_4. d) In-situ C 1s spectra acquired at – 0.1 V and – 0.5 V vs. RHE at the surface of a copper foil immersed in a 1 M H_3PO_4 + 0.01 M FAL electrolyte. e) Atomic percent of C 1s components extracted from in-situ C 1s spectra acquired on copper foil at different potentials in 1 M H_3PO_4 + 0.01 M FAL electrolyte.

than + 0.1 V vs. RHE, they were progressively reduced to Cu(0) and Cu(I) species when scanning to more negative potentials. After adding 0.01 M FAL to the electrolyte, the same experiment was conducted, only this time focusing on analyzing the C 1s signal (because the C 1s signal was masking the Cu 2p signal, it was not possible to monitor both elements at the same time). Quantitative analysis of the C 1s spectra (**Figure 6d-e**) revealed that as the potential was shifted more negatively, the ratio of C-O/C=O increased noticeably between – 0.4 V and – 0.5 V vs. RHE, confirming the reduction of FAL at the surface of the electrode. Interestingly, a peak attributed to

O-C=O moieties, absent from the quasi in-situ experiment reported in **Figure 5**, was identified at all potentials. This was attributed to the oxidation of FAL at the counter-electrode and migration to the working electrode inside the undivided electrochemical cell. Overall this measurement confirmed the observations made on the quasi in-situ experiment performed in the laboratory, and demonstrated the ability of using NAP-XPS for analyzing the composition of the adsorbed organic layer at the surface of the electrode under quasi-operating conditions, providing insight into the catalytic process at the molecular level.

Conclusion

The self-templated copper electrocatalyst presented in this work exhibited much improved activity and selectivity compared to unstructured copper foil. More specifically, studying the influence of temperature and applied potential on the outcome of the electrocatalytic process allowed to identify experimental conditions in which (i) FOH could be selectively produced from FAL in a neutral electrolyte with a 100% FE at unprecedently low overpotential and (ii) either FOH or 2-MF could be selectively produced from FAL in acidic condition, at similarly low overpotentials, albeit with strong HER competition. To better illustrates the latter, **Figure 7** represents the evolution of different metrics as a function of applied potential and temperature measured after 1 hour of FAL reduction in 1 M H_3PO_4. **Figure 7a** shows that there is an optimal combination of temperature and applied potential to promote the conversion of FAL in our setup, namely 40°C and - 0.5 V vs. RHE. Indeed, at more positive voltages and lower temperature, lower current densities resulted in lower conversion rate, while at more negative voltage and higher temperature, HER was increasingly favored over FAL reduction. Moreover, **Figure 7b** clearly shows the existence of two regimes of selectivity, mostly determined by the applied voltage: at potentials more positive than - 0.35 V vs. RHE, FOH was the main product of FAL, while at potentials more negative to this

value, 2-MF was the major product. Importantly, it was found that both products could be selectively obtained in appropriately chosen temperature/voltage domains, although FOH was found to degrade over time in acidic conditions. This was confirmed with the measurement of FE for both products, pictured in **Figure 7c-d**. Importantly, these plots further show that a temperature-voltage optimum exists for 2-MF production, as a result of the optimum

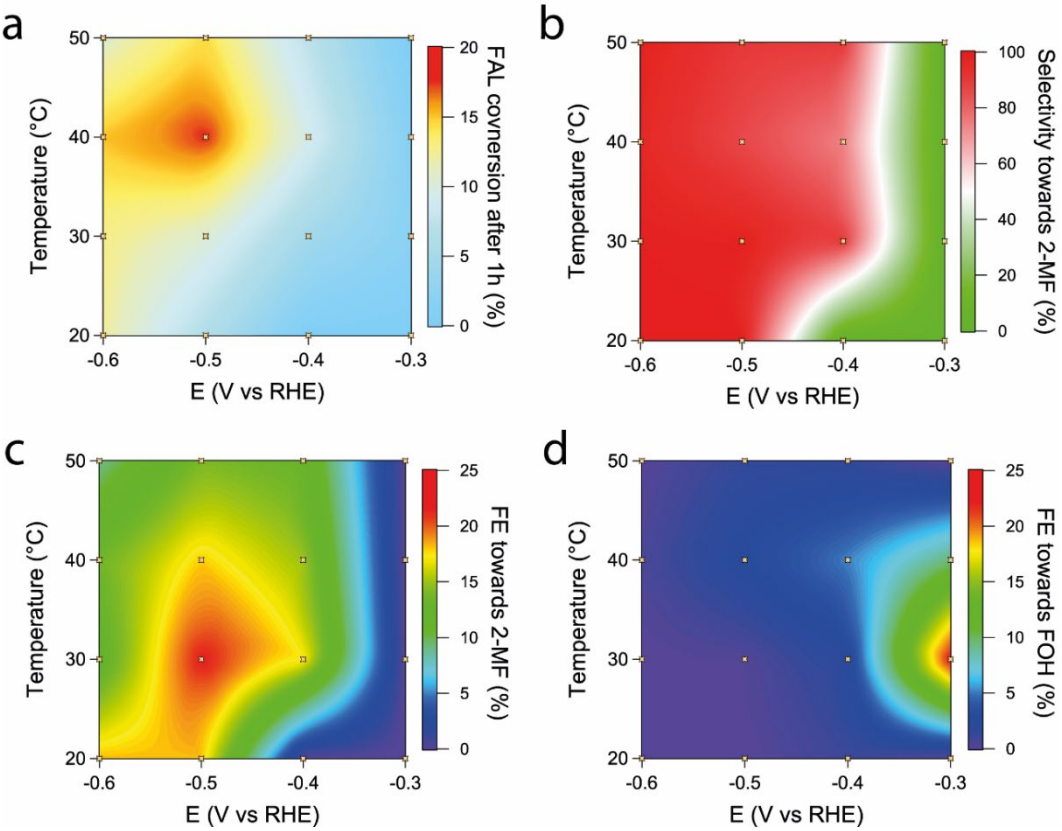

Figure 7 Contour plots of (a) the conversion of FAL, (b) the selectivity of FAL reduction towards 2-MF, the only other conversion product being FOH, (c) the Faradaic efficiency towards FOH production and (d) the Faradaic efficiency towards 2-MF production, as a function of temperature and applied voltage after 1 hour of electrolysis at the surface of a structured Cu electrode in 1 M H_3PO_4 in our electrochemical cell. Markers indicate the experimental data used to plot the figures

in conversion rate and selectivity discussed previously. The existence of this optimum for FAL illustrates the importance of the combined influence of these two driving forces (voltage and

temperature) on the selectivity of complex electrocatalytic processes. Quasi in-situ and in-situ photoelectron spectroscopy was further found to be an insightful tool to shed light on the mechanism of this process, as the analysis of Cu 2p and C 1s signal revealed the resilience of Cu (I) species under operating conditions, as well as a difference in the oxidation state of the organic layer adsorbed at the surface of the electrode, pointing towards differences in the limiting step of electrocatalytic mechanisms between neutral and acidic conditions. While this work demonstrates the benefits of structured Cu electrodes over Cu foil in terms of activity and selectivity, it also showed important competition from the HER in acidic conditions. Experimental and theoretical investigations as well as cell design optimization are under way to understand how to further improve the performance of this system.

ASSOCIATED CONTENT

Supporting Information. The following files are available free of charge.

A PDF containing illustrations of the methods employed in the study, additional SEM data, additional cyclic voltammetry data, complementary activity and selectivity data obtained on structured Cu and Cu foil, activation energy measurements and details on the detection and quantification of dissolved products by HPLC and NMR.

AUTHOR INFORMATION

Corresponding Author

*mathieu.prevot@ircelyon.univ-lyon1.fr

Author Contributions

The manuscript was written through contributions of all authors. All authors have given approval to the final version of the manuscript.

Notes

The authors declare no competing financial interest.

ACKNOWLEDGMENT

We thank the following funding sources for this project: the Marie Skłodowska-Curie action SOLBIOCHEM (project n° 896901), the French National Agency for Research (ANR) project MEGOPE (ANR-22-CE29-0015) and the European Innovation Council (EIC) Pathfinder Project ELOBIO (grant agreement nº 101070856).

We gratefully acknowledge to MAX IV synchrotron for access to HIPPIE beamline through run number 20210958.

We thank the Technological Center on Microstructures of the University of Lyon for access to the Scanning Electron Microscope through their microscopy platform. We also wish to thank the platform IRCATECH platform for acquiring the XRD data shown in this paper.

REFERENCES

(1) Dahmen, N.; Lewandowski, I.; Zibek, S.; Weidtmann, A. Integrated Lignocellulosic Value Chains in a Growing Bioeconomy: Status Quo and Perspectives. *GCB Bioenergy* **2019**, *11* (1), 107–117. https://doi.org/10.1111/gcbb.12586.
(2) Mariscal, R.; Maireles-Torres, P.; Ojeda, M.; Sádaba, I.; Granados, M. L. Furfural: A Renewable and Versatile Platform Molecule for the Synthesis of Chemicals and Fuels. *Energy & Environmental Science* **2016**, *9* (4), 1144–1189. https://doi.org/10.1039/C5EE02666K.
(3) Tang, C.; Zheng, Y.; Jaroniec, M.; Qiao, S.-Z. Electrocatalytic Refinery for Sustainable Production of Fuels and Chemicals. *Angewandte Chemie International Edition* **2021**, *60* (36), 19572–19590. https://doi.org/10.1002/anie.202101522.
(4) Lucas, F. W. S.; Grim, R. G.; Tacey, S. A.; Downes, C. A.; Hasse, J.; Roman, A. M.; Farberow, C. A.; Schaidle, J. A.; Holewinski, A. Electrochemical Routes for the Valorization of Biomass-

Derived Feedstocks: From Chemistry to Application. *ACS Energy Lett.* **2021**, *6* (4), 1205–1270. https://doi.org/10.1021/acsenergylett.0c02692.
(5) Green, S. K.; Lee, J.; Kim, H. J.; Tompsett, G. A.; Kim, W. B.; Huber, G. W. The Electrocatalytic Hydrogenation of Furanic Compounds in a Continuous Electrocatalytic Membrane Reactor. *Green Chem.* **2013**, *15* (7), 1869–1879. https://doi.org/10.1039/C3GC00090G.
(6) Shang, X.; Yang, Y.; Sun, Y. Electrohydrodimerization of Biomass-Derived Furfural Generates a Jet Fuel Precursor. *Green Chem.* **2020**, *22* (16), 5395–5401. https://doi.org/10.1039/D0GC01720E.
(7) Temnikova, M.; Medvedev, J.; Medvedeva, X.; Delva, N. H.; Khairullina, E.; Krivoshapkina, E.; Klinkova, A. Electrochemical Hydrodimerization of Furfural in Organic Media as an Efficient Route to Jet Fuel Precursor. *ChemElectroChem* **2023**, *10* (2), e202200865. https://doi.org/10.1002/celc.202200865.
(8) Albert, W. C.; Lowy, A. The Electrochemical Reduction of Furfural. *Trans. Electrochem. Soc.* **1939**, *75* (1), 367. https://doi.org/10.1149/1.3498392.
(9) Kwon, Y.; Schouten, K. J. P.; van der Waal, J. C.; de Jong, E.; Koper, M. T. M. Electrocatalytic Conversion of Furanic Compounds. *ACS Catal.* **2016**, *6* (10), 6704–6717. https://doi.org/10.1021/acscatal.6b01861.
(10) Li, K.; Sun, Y. Electrocatalytic Upgrading of Biomass-Derived Intermediate Compounds to Value-Added Products. *Chemistry – A European Journal* **2018**, *24* (69), 18258–18270. https://doi.org/10.1002/chem.201803319.
(11) May, A. S.; Biddinger, E. J. Strategies to Control Electrochemical Hydrogenation and Hydrogenolysis of Furfural and Minimize Undesired Side Reactions. *ACS Catal.* **2020**, *10* (5), 3212–3221. https://doi.org/10.1021/acscatal.9b05531.
(12) Wen, H.; Zhang, W.; Fan, Z.; Chen, Z. Recent Advances in Furfural Reduction via Electro- And Photocatalysis: From Mechanism to Catalyst Design. *ACS Catal.* **2023**, 15263–15289. https://doi.org/10.1021/acscatal.3c04372.
(13) Chamoulaud, G.; Floner, D.; Moinet, C.; Lamy, C.; Belgsir, E. M. Biomass Conversion II: Simultaneous Electrosyntheses of Furoic Acid and Furfuryl Alcohol on Modified Graphite Felt Electrodes. *Electrochimica Acta* **2001**, *46* (18), 2757–2760. https://doi.org/10.1016/S0013-4686(01)00507-2.
(14) Parpot, P.; Bettencourt, A. P.; Chamoulaud, G.; Kokoh, K. B.; Belgsir, E. M. Electrochemical Investigations of the Oxidation–Reduction of Furfural in Aqueous Medium: Application to Electrosynthesis. *Electrochimica Acta* **2004**, *49* (3), 397–403. https://doi.org/10.1016/j.electacta.2003.08.021.
(15) Li, Z.; Kelkar, S.; Lam, C. H.; Luczek, K.; Jackson, J. E.; Miller, D. J.; Saffron, C. M. Aqueous Electrocatalytic Hydrogenation of Furfural Using a Sacrificial Anode. *Electrochimica Acta* **2012**, *64*, 87–93. https://doi.org/10.1016/j.electacta.2011.12.105.
(16) zhao, B.; Chen, M.; Guo, Q.; Fu, Y. Electrocatalytic Hydrogenation of Furfural to Furfuryl Alcohol Using Platinum Supported on Activated Carbon Fibers. *Electrochimica Acta* **2014**, *135*, 139–146. https://doi.org/10.1016/j.electacta.2014.04.164.
(17) Chadderdon, X. H.; Chadderdon, D. J.; Matthiesen, J. E.; Qiu, Y.; Carraher, J. M.; Tessonnier, J.-P.; Li, W. Mechanisms of Furfural Reduction on Metal Electrodes: Distinguishing Pathways for Selective Hydrogenation of Bioderived Oxygenates. *J. Am. Chem. Soc.* **2017**, *139* (40), 14120–14128. https://doi.org/10.1021/jacs.7b06331.

(18) Taylor, M. J.; Jiang, L.; Reichert, J.; Papageorgiou, A. C.; Beaumont, S. K.; Wilson, K.; Lee, A. F.; Barth, J. V.; Kyriakou, G. Catalytic Hydrogenation and Hydrodeoxygenation of Furfural over Pt(111): A Model System for the Rational Design and Operation of Practical Biomass Conversion Catalysts. *J. Phys. Chem. C* **2017**, *121* (15), 8490–8497. https://doi.org/10.1021/acs.jpcc.7b01744.

(19) Barranca, A.; Agirrezabal-Tellería, I.; Rellán-Piñeiro, M.; Ortuño, M. A.; Gandarias, I. Selective Furfural Hydrogenolysis towards 2-Methylfuran by Controlled Poisoning of Cu–Co Catalysts with Chlorine. *React. Chem. Eng.* **2023**, *8* (3), 687–698. https://doi.org/10.1039/D2RE00414C.

(20) Jung, S.; Biddinger, E. J. Electrocatalytic Hydrogenation and Hydrogenolysis of Furfural and the Impact of Homogeneous Side Reactions of Furanic Compounds in Acidic Electrolytes. *ACS Sustainable Chem. Eng.* **2016**, *4* (12), 6500–6508. https://doi.org/10.1021/acssuschemeng.6b01314.

(21) Jung, S.; Biddinger, E. J. Controlling Competitive Side Reactions in the Electrochemical Upgrading of Furfural to Biofuel. *Energy Technology* **2018**, *6* (7), 1370–1379. https://doi.org/10.1002/ente.201800216.

(22) Jung, S.; Karaiskakis, A. N.; Biddinger, E. J. Enhanced Activity for Electrochemical Hydrogenation and Hydrogenolysis of Furfural to Biofuel Using Electrodeposited Cu Catalysts. *Catalysis Today* **2019**, *323*, 26–34. https://doi.org/10.1016/j.cattod.2018.09.011.

(23) Anibal, J.; Xu, B. Electroreductive C–C Coupling of Furfural and Benzaldehyde on Cu and Pb Surfaces. *ACS Catal.* **2020**, *10* (19), 11643–11653. https://doi.org/10.1021/acscatal.0c03110.

(24) Zhou, P.; Chen, Y.; Luan, P.; Zhang, X.; Yuan, Z.; Guo, S.-X.; Gu, Q.; Johannessen, B.; Mollah, M.; Chaffee, A. L.; Turner, D. R.; Zhang, J. Selective Electrochemical Hydrogenation of Furfural to 2-Methylfuran over a Single Atom Cu Catalyst under Mild pH Conditions. *Green Chem.* **2021**, *23* (8), 3028–3038. https://doi.org/10.1039/D0GC03999C.

(25) Zhou, P.; Li, L.; Mosali, V. S. S.; Chen, Y.; Luan, P.; Gu, Q.; Turner, D. R.; Huang, L.; Zhang, J. Electrochemical Hydrogenation of Furfural in Aqueous Acetic Acid Media with Enhanced 2-Methylfuran Selectivity Using CuPd Bimetallic Catalysts. *Angewandte Chemie* **2022**, *134* (13), e202117809. https://doi.org/10.1002/ange.202117809.

(26) Xia, Z.; Li, Y.; Wu, J.; Huang, Y.-C.; Zhao, W.; Lu, Y.; Pan, Y.; Yue, X.; Wang, Y.; Dong, C.-L.; Wang, S.; Zou, Y. Promoting the Electrochemical Hydrogenation of Furfural by Synergistic Cu0−Cu+ Active Sites. *Sci. China Chem.* **2022**, *65* (12), 2588–2595. https://doi.org/10.1007/s11426-022-1407-0.

(27) Cui, Y.; Wang, Z.; Li, S. Electrocatalytic Reduction of Furfural for Selective Preparation of 2-Methylfuran over a Trace Ni Assisted Cu Catalyst. *Catal. Sci. Technol.* **2023**, *13* (6), 1846–1854. https://doi.org/10.1039/D3CY00126A.

(28) Liu, S.; Mukadam, Z.; Scott, S. B.; Sarma, S. C.; Titirici, M.-M.; Chan, K.; Govindarajan, N.; Stephens, I. E. L.; Kastlunger, G. Unraveling the Reaction Mechanisms for Furfural Electroreduction on Copper. *EES. Catal.* **2023**, *1* (4), 539–551. https://doi.org/10.1039/D3EY00040K.

(29) Cao, Y.; Noël, T. Efficient Electrocatalytic Reduction of Furfural to Furfuryl Alcohol in a Microchannel Flow Reactor. *Org. Process Res. Dev.* **2019**, *23* (3), 403–408. https://doi.org/10.1021/acs.oprd.8b00428.

(30) Li, Y.; Jia, W.-Z.; Song, Y.-Y.; Xia, X.-H. Superhydrophobicity of 3D Porous Copper Films Prepared Using the Hydrogen Bubble Dynamic Template. *Chem. Mater.* **2007**, *19* (23), 5758–5764. https://doi.org/10.1021/cm071738j.
(31) Plowman, B. J.; Jones, L. A.; Bhargava, S. K. Building with Bubbles: The Formation of High Surface Area Honeycomb-like Films via Hydrogen Bubble Templated Electrodeposition. *Chem. Commun.* **2015**, *51* (21), 4331–4346. https://doi.org/10.1039/C4CC06638C.
(32) Pérez Sánchez, M.; Barrera, M.; González, S.; Souto, R. M.; Salvarezza, R. C.; Arvia, A. J. Electrochemical Behaviour of Copper in Aqueous Moderate Alkaline Media, Containing Sodium Carbonate and Bicarbonate, and Sodium Perchlorate. *Electrochimica Acta* **1990**, *35* (9), 1337–1343. https://doi.org/10.1016/0013-4686(90)85004-7.
(33) Long, J.; Zhao, W.; Xu, Y.; Wu, W.; Fang, C.; Li, H.; Yang, S. Low-Temperature Catalytic Hydrogenation of Bio-Based Furfural and Relevant Aldehydes Using Cesium Carbonate and Hydrosiloxane. *RSC Advances* **2019**, *9* (6), 3063–3071. https://doi.org/10.1039/C8RA08616H.
(34) Durndell, L. J.; Parlett, C. M. A.; Hondow, N. S.; Isaacs, M. A.; Wilson, K.; Lee, A. F. Selectivity Control in Pt-Catalyzed Cinnamaldehyde Hydrogenation. *Sci Rep* **2015**, *5* (1), 9425. https://doi.org/10.1038/srep09425.
(35) An, W.; Men, Y.; Wang, J. Comparative Study on Hydrogenation of Propanal on Ni(111) and Cu(111) from Density Functional Theory. *Applied Surface Science* **2017**, *394*, 333–339. https://doi.org/10.1016/j.apsusc.2016.10.064.
(36) Song, Y.; Sanyal, U.; Pangotra, D.; Holladay, J. D.; Camaioni, D. M.; Gutiérrez, O. Y.; Lercher, J. A. Hydrogenation of Benzaldehyde via Electrocatalysis and Thermal Catalysis on Carbon-Supported Metals. *Journal of Catalysis* **2018**, *359*, 68–75. https://doi.org/10.1016/j.jcat.2017.12.026.
(37) Gengenbach, T. R.; Major, G. H.; Linford, M. R.; Easton, C. D. Practical Guides for X-Ray Photoelectron Spectroscopy (XPS): Interpreting the Carbon 1s Spectrum. *Journal of Vacuum Science & Technology A: Vacuum, Surfaces, and Films* **2021**, *39* (1), 013204. https://doi.org/10.1116/6.0000682.
(38) Zhu, S.; Scardamaglia, M.; Kundsen, J.; Sankari, R.; Tarawneh, H.; Temperton, R.; Pickworth, L.; Cavalca, F.; Wang, C.; Tissot, H.; Weissenrieder, J.; Hagman, B.; Gustafson, J.; Kaya, S.; Lindgren, F.; Källquist, I.; Maibach, J.; Hahlin, M.; Boix, V.; Gallo, T.; Rehman, F.; D'Acunto, G.; Schnadt, J.; Shavorskiy, A. HIPPIE: A New Platform for Ambient-Pressure X-Ray Photoelectron Spectroscopy at the MAX IV Laboratory. *J Synchrotron Rad* **2021**, *28* (2), 624–636. https://doi.org/10.1107/S160057752100103X.

Graphical abstract: